nature structural & molecular biology

Allosteric opening of the polypeptide-binding site when an Hsp70 binds ATP

Ruifeng Qi[1,5], Evans Boateng Sarbeng[1,5], Qun Liu[2,5], Katherine Quynh Le[1,5], Xinping Xu[1], Hongya Xu[1], Jiao Yang[1], Jennifer Li Wong[1], Christina Vorvis[1], Wayne A Hendrickson[2–4], Lei Zhou[1] & Qinglian Liu[1]

The 70-kilodalton (kDa) heat-shock proteins (Hsp70s) are ubiquitous molecular chaperones essential for cellular protein folding and proteostasis. Each Hsp70 has two functional domains: a nucleotide-binding domain (NBD), which binds and hydrolyzes ATP, and a substrate-binding domain (SBD), which binds extended polypeptides. NBD and SBD interact little when in the presence of ADP; however, ATP binding allosterically couples the polypeptide- and ATP-binding sites. ATP binding promotes polypeptide release; polypeptide rebinding stimulates ATP hydrolysis. This allosteric coupling is poorly understood. Here we present the crystal structure of an intact ATP-bound Hsp70 from *Escherichia coli* at 1.96-Å resolution. The ATP-bound NBD adopts a unique conformation, forming extensive interfaces with an SBD that has changed radically, having its α-helical lid displaced and the polypeptide-binding channel of its β-subdomain restructured. These conformational changes, together with our biochemical assays, provide a structural explanation for allosteric coupling in Hsp70 activity.

Maintaining protein homeostasis (proteostasis) is a fundamental task for all living organisms, and in humans, failure to do so contributes to destructive diseases, such as cancers and neurodegenerative disorders[1,2]. By assisting protein folding, assembly, degradation and transport across membranes, the Hsp70 proteins are key players in proteostasis.

Hsp70s are highly conserved. Each contains two functional domains, an NBD and an SBD, which are joined by a short linker segment[3–5] (**Fig. 1a**). NBD is an ATPase and SBD substrates are extended hydrophobic polypeptides like those that occur in unfolded proteins[6]. The first NBD structure was of NBD isolated from bovine Hsc70, which has ADP bound at a site between two lobes[7] (lobe I and lobe II), and all subsequent Hsp70 structures have been either ADP-bound or nucleotide-free[8–11]. The first SBD structure was of the SBD isolated from the *E. coli* Hsp70 DnaK in complex with a short peptide[12]. Other known SBD structures have essentially the same conformation[10,11,13–15], with the polypeptide-binding site more dynamic in solution in the absence of peptide substrate[14].

Although NBD and SBD can each bind its substrate independently, the chaperone activity of Hsp70s strictly requires tight coupling of these two domains upon ATP binding. Various biochemical and structural studies, mainly of DnaK as a model Hsp70, have shown that in ADP-bound or nucleotide-free states there is little contact between NBD and SBD; each domain acts independently as though isolated[11,16–18]. In contrast, upon ATP binding, the affinity of SBD for its substrates is reduced by two to three orders of magnitude[19,20]. Rates of both binding and release are greatly accelerated, but release is more so than binding. Reciprocally, polypeptide binding to SBD stimulates ATP hydolysis[3,20]. This allosteric coupling ensures that energy from ATP hydrolysis is efficiently used to control peptide substrate binding and release for efficient chaperone activity. Despite extensive efforts, the basic mechanism of this ATP-induced allosteric coupling is still poorly defined.

Crystal structures of full-length Hsp70s containing both functional domains in the ATP-bound state have been highly sought in anticipation of insight into Hsp70 allostery. This goal has proven challenging, however, because of ATP lability and the transience of allosteric coupling. In fact, even structures of isolated ATP-bound NBDs are elusive[7,8,21,22]. Hsp110s are distant homologs of Hsp70s, and our structure of ATP-bound Sse1 (Sse1-ATP), a yeast Hsp110, provided an invaluable starting point for mechanistic understanding of allosteric coupling in Hsp70s (refs. 4,5,23–27); however, its applicability to Hsp70s is limited, owing to relatively low sequence conservation, especially between SBD regions[23]. To explore the molecular mechanism of this essential ATP-induced allosteric coupling, we solved a crystal structure of an intact Hsp70 from *E. coli* in complex with ATP. Our biochemical analysis inspired by this structure provides a mechanistic understanding of how ATP binding allosterically opens the polypeptide-binding site.

RESULTS

Hsp70 DnaK locked in an ATP-bound state

To study a functionally complete Hsp70 in the ATP-bound state, we incorporated two previously reported mutations into *E. coli* DnaK:

[1]Department of Physiology and Biophysics, Virginia Commonwealth University, Richmond, Virginia, USA. [2]New York Structural Biology Center, X4 Beamlines, Brookhaven National Laboratory, Upton, New York, USA. [3]Department of Biochemistry and Molecular Biophysics, Columbia University, New York, New York, USA. [4]Department of Physiology and Cellular Biophysics, Columbia University, New York, New York, USA. [5]These authors contributed equally to this work. Correspondence should be addressed to Qinglian Liu (qliu3@vcu.edu).

Received 6 February; accepted 8 April; published online 26 May 2013; doi:10.1038/nsmb.2583

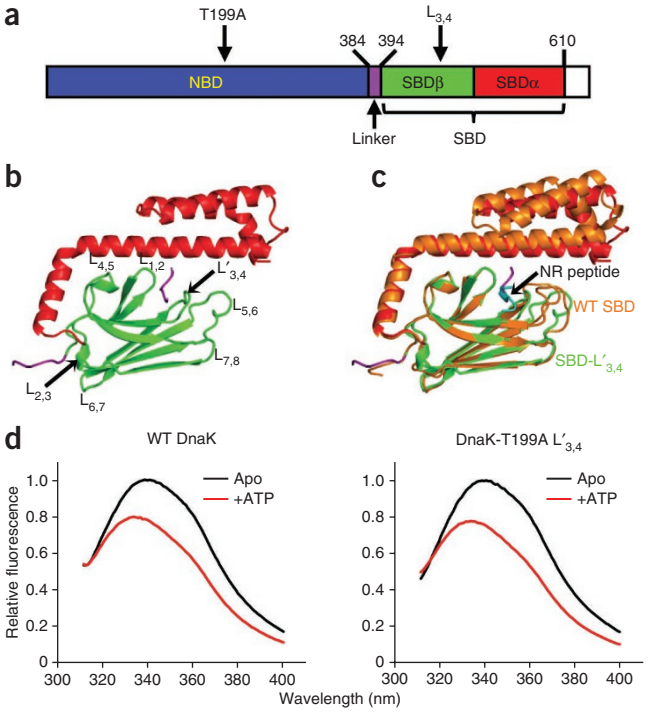

Figure 1 Characteristics of DnaK locked in an ATP-bound state. (**a**) Schematic of Hsp70 domain structure, including NBD (blue), linker (purple), SBDβ (green) and SBDα (red). Positions of key elements are indicated. (**b**) Ribbon representation of the DnaK SBD-$L'_{3,4}$ structure. Domain color assignments are as in **a**. The linker segment from a symmetry mate (purple) binds to the polypeptide-binding site between $L_{1,2}$ and $L'_{3,4}$. (**c**) Superposition of SBDβ from the DnaK SBD-$L'_{3,4}$ structure (color assignments as in **a**) with that of the wild-type (WT) SBD structure (orange; PDB 1DKZ). The peptide substrate NR in the WT SBD structure is shown (cyan). (**d**) Tryptophan-fluorescence emission spectra for assaying the ATP-induced allosteric coupling of DnaK.

T199A and loop $L_{3,4}$ alternative $L'_{3,4}$ (**Fig. 1a** and **Supplementary Fig. 1**). T199A is a well-characterized mutation that abolishes ATPase activity but maintains allosteric coupling[16,28]; it helped to stabilize Hsp70 in a relevant ATP-bound state. DnaK tends to self-associate into flexible oligomers[29], which complicates crystallization. Recently, we produced a peptide-binding–deficient DnaK mutant in which peptide-binding loop $L_{3,4}$ was replaced by a shortened $L_{1,2}$ sequence (TAEDNQS→MGG)[30]; this modification solved the self-association problem. Furthermore, to facilitate crystallization, we removed 28 residues at the extreme C-terminal region, which is disordered[18,31]. The resulting construct was designated DnaK-T199A $L'_{3,4}$.

To investigate the structural impact of the $L'_{3,4}$ modification, we solved the crystal structure of an isolated SBD variant of DnaK carrying this modification (SBD-$L'_{3,4}$) at 1.62-Å resolution (**Fig. 1b** and **Table 1**). SBD comprises two subdomains: SBDβ forms a single polypeptide-binding channel between loops $L_{1,2}$ and $L_{3,4}$, and SBDα functions as a lid covering the polypeptide-binding site on SBDβ[12] (**Fig. 1c**). A short model peptide substrate (NRLLLTG) is bound in the polypeptide-binding site in the isolated wild-type SBD structure. Except for the shortening of $L_{3,4}$ by four residues, SBD-$L'_{3,4}$ is almost identical to the previously solved wild-type SBD structure[12] (0.45 Å r.m.s. deviation in SBDβ Cα atoms). SBDα is rotated slightly (**Fig. 1c**), consistent with the intrinsic flexibility of this region[12,15]. Substrate peptides bind too weakly to the DnaK protein carrying the $L'_{3,4}$ mutation (DnaK-$L'_{3,4}$) to be detected by fluorescence anisotropy assays[30]; however, the linker segment from a symmetry mate binds to SBD-$L'_{3,4}$ at the high concentrations in crystals, similarly to how the model peptide binds wild-type SBD (**Fig. 1b**,**c**).

To investigate the functional impact of the T199A and $L'_{3,4}$ mutations, we used a well-established tryptophan fluorescence assay of allosteric coupling. DnaK has a single tryptophan, Trp102 in NBD, whose intrinsic fluorescence emission spectrum is sensitive to the nucleotide-binding state. Relative to the apo and ADP-bound forms, ATP binding induces blueshift and fluorescence quenching, but only in the context of full-length DnaK when there is allosteric coupling[16]. Tryptophan-fluorescence changes upon ATP addition were almost identical for DnaK-T199A $L'_{3,4}$ as for wild-type DnaK (**Fig. 1d**). Thus, this variant has a wild-type–like conformation in the ATP-bound state.

Crystals of DnaK-T199A $L'_{3,4}$ grew only in the presence of ATP. Hereafter, we refer to the complex as DnaK-ATP. The crystals diffract well and have two DnaK chains per asymmetric unit (**Table 1**). We solved the structure by multi-crystal native single-wavelength anomalous diffraction (SAD)[32]. Resulting electron density maps were of high quality, showing well-defined Mg^{2+}-ATP ligands (**Supplementary Fig. 2**) and allowing automated model building. Separately collected native data were used for refinement at 1.96-Å resolution. The final model had excellent stereochemistry (no Ramachandran outliers).

The two crystallographically unique DnaK-ATP protomers were almost identical (Cα r.m.s. deviation = 0.40 Å; all-atom r.m.s. deviation = 0.82 Å), related by near-dyad symmetry (rotation $\chi = 179.9°$; translation $t_\chi = 0.15$Å) (**Fig. 2a**). Each protomer was composed of familiar NBD, linker, SBDβ and SBDα domains and ATP; however, domains were disposed uniquely (**Fig. 2b**) with extensive interfaces and unanticipated conformational changes. Thus, the DnaK-ATP structure gives a first view of a full-length, ATP-bound Hsp70.

Comparison to Hsp70-ADP and Hsp110-ATP

The DnaK-ATP structure is radically different from ADP-bound and nucleotide-free Hsp70 structures[10,11,18], wherein NBD and SBD are mostly independent, both structurally and functionally; however, it shares similarities with the Sse1-ATP structure. NMR analysis of DnaK-ADP showed a distribution of orientations for SBD relative to NBD and produced an average solution structure using X-ray crystal structures for the domains[18] (**Fig. 2c**).

Various biochemical and NMR studies have suggested that NBD and SBD contact one another in the presence of ATP[3–5,16,17,33]. Consistent with these observations, we found numerous contacts between domains of DnaK-ATP (**Fig. 2b**), which involve substantial conformational change within the NBD and the SBD. In summary, SBDα is peeled away from the polypeptide-binding site on SBDβ, as seen in the isolated SBD structure (and adopted in the DnaK-ADP model)[18]. SBDα docks onto the lobe I side of NBD, and subdomain SBDβ binds between lobe I and lobe II at the lower backside (in the canonical view) of NBD (**Fig. 2b**). The two lobes of NBD move apart such that the linker fits into the cleft between them; and, consistent with its essential role in allosteric coupling[17,34–36], the linker then extends directly into SBDβ. Thus, the overall conformation of DnaK-ATP was completely different from that of DnaK-ADP (**Fig. 2c**).

The NBD-SBD interfaces and the relative orientation of the domains in DnaK-ATP agree well with many previous biochemical and biophysical studies, including a number of recent studies using NMR and FRET[24–27,35–37]. Notably, this structure provides a direct explanation for the well-established tryptophan-fluorescence shifts that accompany ATP-induced allosteric coupling in DnaK[16]. The Sse1-ATP structure already hinted at this explanation, but the

Table 1 Data collection and refinement statistics

	DnaK SBD-L′$_{3,4}$ (native)	DnaK-ATP (native)	DnaK-ATP (SAD)
Data collection			
Space group	$P3_121$	$I422$	$I422$
Cell dimensions			
a, *b*, *c* (Å)	67.0, 67.0, 128.8	290.7, 290.7, 99.3	291.7, 291.7, 99.5
α, β, γ (°)	90, 90, 120	90, 90, 90	90, 90, 90
Resolution (Å)[a]	30–1.62 (1.65–1.62)	30–1.96 (2.01–1.96)	30–2.30 (2.36–2.30)
No. reflections	381,376	1,204,143	12,331,244
R_{merge}[a]	0.047 (0.261)	0.070 (0.358)	0.125 (0.498)[b]
$I / \sigma I$[a]	54.0 (5.1)	21.7 (5.1)	64.5 (16.2)
Completeness (%)[a]	98.9 (86.8)	99.8 (97.4)	100.0 (100.0)
Redundancy[a]	8.9 (5.0)	8.0 (5.8)	148.5 (87.1)
Refinement			
Resolution (Å)[a]	30–1.62 (1.66–1.62)	30–1.96 (1.98–1.96)	30–2.30 (2.33–2.30)
No. unique reflections	42,464	150,429	182,212
R_{work} / R_{free}	0.191 / 0.216	0.172 / 0.201	0.164 / 0.197
No. atoms	1,923	10,677	10,366
Protein	1,600	9,100	9,100
Ligand/ion	–	118 / 62	118 / 62
Water	323	1,397	1,086
Average *B*-factors (Å^2)	28.9	32.5	32.4
Protein	27.2	31.4	31.7
Ligand/ion	–	42.1	35.2
Water	37.5	39.4	38.1
r.m.s. deviations			
Bond lengths (Å)	0.006	0.005	0.005

One crystal was used for each native data set, and five crystals were used for the SAD data set.
[a]Values in parentheses are for the highest-resolution shell. [b]R_{meas} as reported by program SCALA.

NBD-SBDα interface of DnaK-ATP actually has SBDα residues Leu507 and Met515 directly contacting Trp102 (**Supplementary Fig. 3a**); in ADP-bound or nucleotide-free states, Trp102 is exposed. This more hydrophobic environment for Trp102 explains the spectral shift and quenching upon ATP binding. In addition, cysteine residues introduced strategically at structure-inspired NBD-SBDα interfaces formed disulfide bonds specifically in the presence of ATP (**Supplementary Fig. 3**), supporting the existence of a crystal-like conformation of DnaK-ATP in solution.

As much as DnaK-ATP differs from DnaK-ADP (and related Hsp70 structures), it was similar to Sse1-ATP (**Fig. 2d**). This was expected from biochemical analyses of the yeast Hsp110 structure, Sse1-ATP[23], and it supports the hypothesis that Sse1-ATP is an evolutionary vestige of the Hsp70-ATP state[23] with some shared characteristics of allosteric coupling[30]. Most notably, we found that the linker disposition is highly conserved between the two structures (**Supplementary Fig. 4a**). Although DnaK-ATP and Sse1-ATP are superficially similar, there are many important differences. When the NBDs are aligned, both SBDα and SBDβ were rotated substantially in DnaK compared to Sse1, by 41.8° and 24.0°, respectively (**Fig. 2d**), owing to marked changes in the NBD-SBDα and NBD-SBDβ domain interfaces. The most remarkable difference between DnaK-ATP and Sse1-ATP was in the conformation of SBDβ (**Supplementary Fig. 4b**). Furthermore, SBDα in DnaK-ATP was also rotated 45.1°, relative to its SBDβ.

ATP-elicited opening of the polypeptide-binding site

DnaK, when bound to ATP, assumes a markedly different conformation than that seen in any other Hsp70 structure that we know of, with respect to both NBD and SBD. Changes initiate at the ATP-binding site, propagate through NBD to interfaces for linker and SBD subdomains and transform SBDβ into a state that releases its polypeptide substrate. Other Hsp70 NBD structures have been in either the ADP-bound or the nucleotide-free state[4,5,7–11,21], and NBD of DnaK-ATP was substantially different from those (**Fig. 3a**). It does resemble the ATP-bound conformation of Sse1-ATP[23] (Cα r.m.s. deviation = 1.54 Å; **Fig. 3b**). Indeed, the Mg^{2+}-ATP complexes were virtually identical in the two structures (**Supplementary Fig. 4c**). ATP interacts intimately with DnaK, contacting 24 residues, 21 of which are identical across a range of Hsp70s (**Supplementary Fig. 1**). When modeled into the structure, the hydroxyl group of Thr199 played a part in ATP hydrolysis. Upon ATP binding, consistent with NMR studies[35,37], lobe I rotates by 25.5° relative to lobe II, as seen in a comparison between DnaK-ATP and human Hsp70-ADP (**Fig. 3a**). This rotation opens a slot between DnaK subdomains IA and IIA that binds the linker segment; however, this linker binding can accommodate SBD only when SBDα is displaced from SBDβ (**Supplementary Fig. 4d**).

The highly conserved DVLLLD linker segment of DnaK runs directly into SBD, whereby the proximate end of SBDβ interacts intimately with NBD. Interfacial contacts made from loops $L_{L,1}$, $L_{2,3}$ and $L_{4,5}$ of SBD keep the ADP-state conformation of the isolated SBD-peptide complex[12] (**Fig. 3c** and **Supplementary Fig. 4d–f**); in contrast, contacts mediated by $L_{6,7}$ and $L_{\alpha,\beta}$ generated substantial movements in those loops and in β8 relative to the fixed base (**Fig. 3c**). These changes happen as SBDα is separated from SBDβ (**Supplementary Fig. 4d–f**). Helices αA and αB of SBDα (as seen in isolated SBD) fuse into one long helix that binds alongside NBD lobe I (**Supplementary Fig. 4e**), and this displacement 'pulls' $L_{\alpha,\beta}$ upward (**Fig. 3c**), moving strand β8 from the lower to the upper β-sheet. $L_{6,7}$ also moves (although its conformation does not change; **Supplementary Fig. 4g**) against the fixed fulcrum of the $L_{L,1}$, $L_{2,3}$ and $L_{4,5}$ contacts, appearing to exert a torque that 'pushes' distal elements of SBDβ outward and downward. As a result, the β-sandwich of the SBDβ domain in DnaK-ATP was twisted relative to that in the SBD-peptide complex (**Fig. 3c**) such that the distal loops (both the shortened L′$_{3,4}$ and $L_{5,6}$) projected from the β-strand core, out and away from the peptide-binding site (**Fig. 3c**,**d**). As a consequence of these changes, the polypeptide-binding channel is flipped open on the distal side, with shifts of up to 22.8 Å (Cα of Arg467 in $L_{5,6}$). The proximal side of the binding site, $L_{1,2}$ and $L_{4,5}$, showed very little change. In the isolated SBD-peptide structure, Leu3, Leu4 and Leu5 of the model peptide reside in the center of the polypeptide-binding site, mediating numerous van der Waals contacts[12] (**Fig. 3d**). The flipping open of L′$_{3,4}$ and $L_{5,6}$ in DnaK-ATP abolished contacts from that side of the binding site (**Fig. 3d**). Thus, the SBDβ conformation in DnaK-ATP matches well with the reduced peptide affinity, and accelerated binding and dissociation rates in ATP-bound Hsp70s. This ATP-bound conformation of L′$_{3,4}$ and $L_{5,6}$ is also consistent with

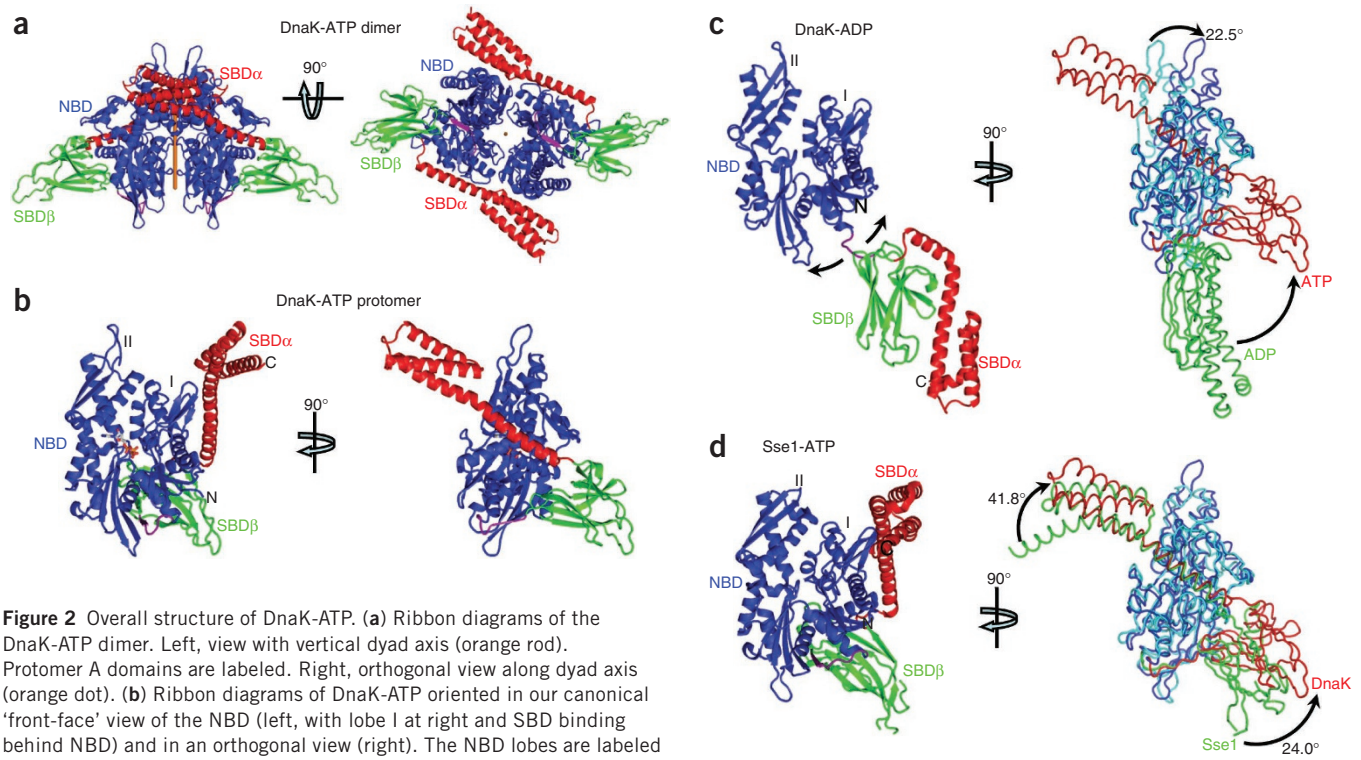

Figure 2 Overall structure of DnaK-ATP. (**a**) Ribbon diagrams of the DnaK-ATP dimer. Left, view with vertical dyad axis (orange rod). Protomer A domains are labeled. Right, orthogonal view along dyad axis (orange dot). (**b**) Ribbon diagrams of DnaK-ATP oriented in our canonical 'front-face' view of the NBD (left, with lobe I at right and SBD binding behind NBD) and in an orthogonal view (right). The NBD lobes are labeled (I and II). The bound ATP molecule is shown as a stick representation. (**c**) Comparison of DnaK-ADP with DnaK-ATP. Left, ribbon diagram of the DnaK-ADP structure in the front-face NBD view (PDB 2KHO). Right, orthogonal view of DnaK-ATP in backbone worm representation as superimposed onto DnaK-ADP on the basis of NBD lobe I Cα positions. Shown are NBD from DnaK-ATP (blue), SBD from DnaK-ATP (red), NBD from DnaK-ADP (cyan) and SBD from DnaK-ADP (green). (**d**) Comparison of Sse1-ATP with DnaK-ATP. Left, ribbon diagram of the Sse1-ATP structure in the front-face NBD view (PDB 2QXL). Right, orthogonal view of DnaK-ATP in backbone worm representation as superimposed onto Sse1-ATP on the basis of NBD lobe I Cα positions. Domain color assignments for DnaK-ATP are as in **c**; Sse1-ATP NBD is shown in blue and Sse1-ATP SBD in green.

increased solvent accessibility of these loops in solution[17,38]. This conformational change that accompanies ATP binding to DnaK, whereby the polypeptide-binding channel is opened, could be the structural basis for allosteric coupling in Hsp70 chaperones generally.

Consistent with the DnaK-ATP structure, an NMR study of isolated apo-SBDβ, DnaK (393–507) without peptide substrate, has shown that peptide-binding loops $L_{3,4}$ and $L_{5,6}$ are flexible and dynamic[14]. $L_{3,4}$ and $L_{5,6}$ in the NMR structure of apo-SBDβ were positioned somewhere in between their positions in the DnaK-ATP and isolated SBD-peptide structures (**Supplementary Fig. 5a–d**). The polypeptide-binding loops in DnaK-ATP made contacts with symmetry mates in the crystal lattice (**Supplementary Fig. 5e,f**). Thus, it is possible that loops $L_{3,4}$ and $L_{5,6}$ are dynamic in the ATP-bound state, as in isolated apo-SBDβ, and that lattice contacts stabilize a flipped-out member of an ensemble of ATP-bound conformations. To estimate how much crystal contacts might have affected the conformation of these loops, we carried out molecular dynamic simulations without crystal contacts, and found that SBDβ was the most stable element in the DnaK-ATP structure and was much more stable than other SBDβ structures; apo-SBDβ was the least stable (**Supplementary Fig. 5g**). Stabilizing contacts permeate the β-strands of SBDβ in DnaK-ATP, which differed markedly from those in the isolated SBD structure[12] (**Fig. 3c**). Loops $L_{3,4}$ and $L_{5,6}$ emanated in an opened trajectory from these strands as stabilized by NBD-SBD interfaces, and we conclude that flexibility is limited to tips of the loops. Disulfide cross-linking experiments confirmed that DnaK-ATP in solution is similar to the crystal structure (**Supplementary Fig. 3**). Thus, NBD-SBD interfaces generated upon binding of ATP fix the bases of $L_{3,4}$ and $L_{5,6}$ in SBDβ in an open conformation that is incompatible with strong peptide binding. The tips of loops may remain flexible, consistent with previous NMR studies[14,39]; however, unlike those of apo or peptide-bound SBDβ domains, the ensemble of states for DnaK-ATP is predisposed toward open conformations.

Conformational impact of conserved glycine residues on $L_{5,6}$

To test the hypothesis that the opening of the polypeptide-binding channel upon ATP binding could be responsible for polypeptide release, we examined residues on $L_{5,6}$. We found that two highly conserved residues, Gly461 and Gly468, changed backbone conformations dramatically (**Fig. 4a** and **Supplementary Fig. 1**), whereas other residues showed only moderate changes. We made glycine-to-proline mutations G461P and G468P because proline residues allow the phi and psi conformational angles of DnaK-ATP but not of isolated SBD[40], the ADP state (**Fig. 2c**); thus, these mutants are designed to locally restrict SBDβ to its conformation in the ATP-bound state independent of ATP-induced domain contacts. Mutation of either glycine residue individually compromised *in vivo* DnaK function modestly, but mutation of both (DnaK-PP) abolished DnaK function (**Fig. 4b** and **Supplementary Fig. 6a**), despite wild-type levels of expression (**Supplementary Fig. 6e**). Tests with yeast Hsp70 Ssa1 gave similar results, suggesting a universal importance in Hsp70s (**Fig. 4b** and **Supplementary Fig. 6a**).

To test impact of the DnaK-PP mutation on specific characteristics of DnaK activity, we purified the mutant protein for *in vitro* activity assays. We found that the chaperone activity of wild-type DnaK in refolding

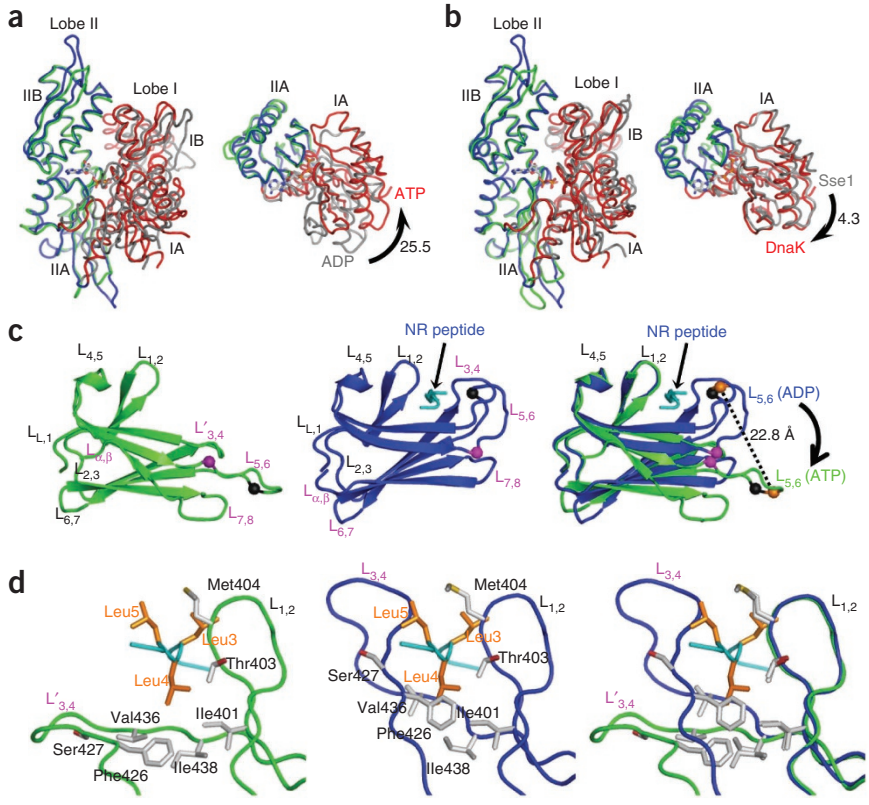

Figure 3 Unique conformations of NBD and SBD in DnaK-ATP. (**a**) Comparison of NBD domains in DnaK-ATP and human Hsp70-ADP (1S3X) as superimposed on the basis of Cαs in lobe II. Left, canonical 'front-face' view; right, top view of the left panel with subdomains IB and IIB removed to show the changes in IA and IIA. For DnaK-ATP, lobe I is shown in red and lobe II is in blue; for human Hsp70-ADP, lobe I is shown in gray, and lobe II is in green. (**b**) Comparison of DnaK-ATP and Sse1-ATP. Superpositions and color-coding are as in **a**, except that Sse1-ATP replaces human Hsp70-ADP. (**c**) Comparison of SBDβ conformations. Ribbon diagrams are drawn for SBDβs from DnaK-ATP (left), isolated DnaK-SBD (PDB 1DKZ; middle), and their superposition (right). SBDβs were superimposed based on Cαs in $L_{1,2}$ and $L_{4,5}$. Cα atoms of Gly461 (purple spheres), Arg467 (orange spheres), and Gly468 (black spheres) on loop $L_{5,6}$ are highlighted. NR peptide is shown in cyan. (**d**) Comparison of polypeptide-binding sites. Polypeptide-binding sites are drawn for DnaK-ATP (left; NR peptide is from the isolated DnaK-SBD structure), isolated DnaK-SBD (middle), and their superposition (right). The structures were superimposed based on the Cαs in $L_{1,2}$ and $L_{4,5}$. The backbones of DnaK-ATP (green), DnaK-SBD (blue) and NR peptide (cyan) are drawn as backbone worms. SBD side chains that make van der Waals contacts with NR side chains of Leu3, Leu4 and Leu5 (orange) are shown as stick drawings.

of heat-denatured luciferase is lost for the DnaK-PP mutant (**Fig. 4c**). Moreover, we found that peptide binding to DnaK-PP is aberrant. Unlike the wild-type protein in the presence of ADP or the absence of nucleotides, where binding affinity is high and binding kinetics are slow, DnaK-PP bound substrate peptides with reduced affinity (**Fig. 4d**) and fast binding kinetics (**Fig. 4e**), as happens for wild-type DnaK in ATP[19]. DnaK-PP underwent normal ATP-induced NBD-SBD associations as measured by tryptophan fluorescence. These results are consistent with the hypothesis that SBDβ of DnaK-PP is locked locally into an ATP-like conformation, irrespectively of the ATP or ADP status of the NBD. Thus, the two $L_{5,6}$ glycine residues are crucial for ATP-induced conformational changes in SBDβ. In summary, our results from molecular dynamic simulations, disulfide cross-linking and the DnaK-PP mutant analysis suggest that a flipped-out conformation of $L_{3,4}$ and $L_{5,6}$ in DnaK-ATP is physiologically important even though crystal contacts may stabilize one of an ensemble of states.

Domain interfaces in allosteric coupling

The unique conformation of DnaK-ATP arises from extensive interfaces that form between domains as they adapt to ATP binding. There are three major interdomain contacts: NBD-linker, NBD-SBDβ and NBD-SBDα (**Fig. 2b**). The interfacial surfaces are conserved among Hsp70s (**Fig. 5**), and especially so in the crucial NBD-SBDβ interface. SBDβ has additional conservation at the polypeptide-binding channel (**Fig. 5b**). Large surface areas are buried in the interfaces; however, shape complementarity is low compared to similar

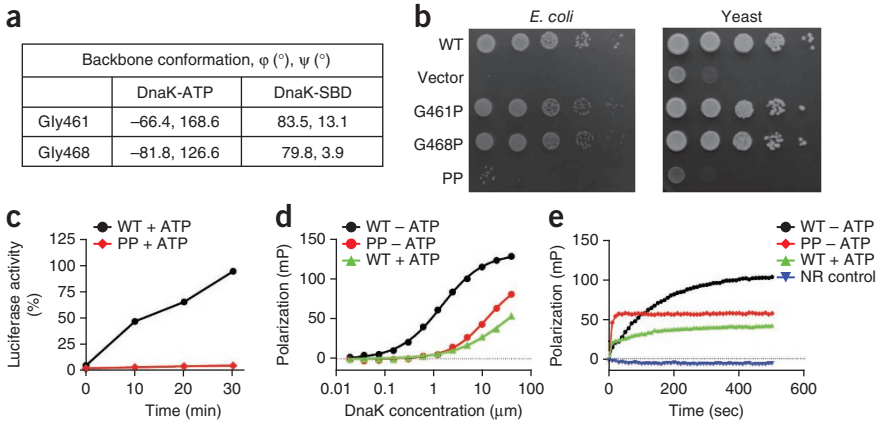

Figure 4 Two highly conserved glycine residues in $L_{5,6}$. (**a**) Comparison of phi (φ) and psi (ψ) angles for Gly461 and Gly468 in DnaK-ATP and isolated DnaK-SBD structures. (**b**) Growth tests for glycine mutants in Hsp70-deficient *E. coli* and yeast backgrounds. Serial dilutions (10× column-by-column) of fresh cultures were spotted onto plates and incubated at 37 °C. (**c**) Activity in refolding of heat-denatured luciferase by wild-type (WT) and G461P G468P mutant DnaK (PP) in the presence of ATP (+ATP). (**d**) Fluorescence anisotropy assay of peptide substrate binding affinity. Serial dilutions of DnaK proteins were incubated with F-NR, a model peptide substrate, in the presence (+) or absence (–) of ATP. Fluorescence anisotropy measurements were made after binding reached equilibrium. (**e**) Peptide substrate binding kinetics determined by fluorescence anisotropy assay. Peptide binding as a function of time was measured immediately after mixing DnaK with the F-NR peptide.

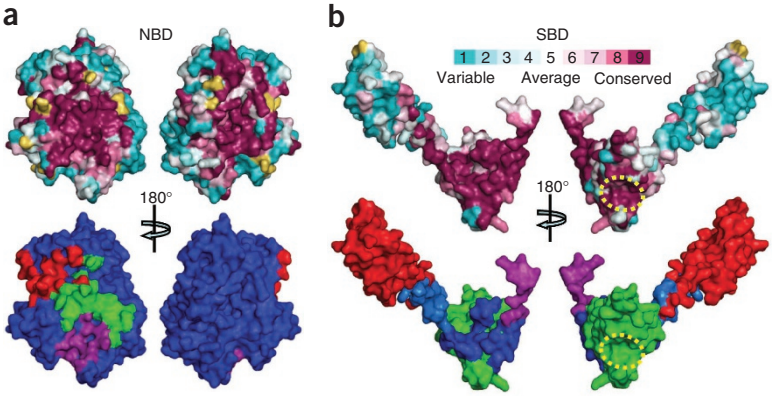

Figure 5 Sequence conservation at domain interfaces in DnaK-ATP. (**a**,**b**) Sequence conservation at the surface of NBD (**a**, top) and SBD (**b**, top). Conservation surface mappings are as reported by ConSurf (http://consurf.tau.ac.il/) and coded by the key. The polypeptide-binding site is indicated (**b**, dotted yellow line). Mappings of domain interfaces onto the surfaces of NBD (**a**, bottom) and SBD (**b**, bottom) are shown. In **a**, the surface of NBD is shown in blue, and the imprints of contacts are color-coded by domain: SBDα (red), SBDβ (green), linker (purple). In **b**, the surfaces of linker, SBDβ and SBDα are shown in purple, green and red, respectively, and the imprints of contacts from NBD are color-coded according to the subdomain receiving that contact: SBDβ (blue), SBDα (aquamarine) and linker (purple, as it is buried in the interface with NBD).

interfaces in Sse1-ATP (**Supplementary Table 1**), which might relate to the transient nature of allosteric coupling in Hsp70s.

The NBD-SBD interaction in DnaK-ATP originates at the linker segment connecting the two domains, and it involves intimate contacts between both the linker-proximate end of the SBDβ β-sandwich and the displaced SBDα α-helical lid as in Sse1-ATP (**Fig. 6a** and **Supplementary Fig. 7a**,**b**). Besides its contacts to the linker and SBDα, NBD also interacts with the three proximate SBDβ loops that join β-strands ($L_{2,3}$, $L_{4,5}$ and $L_{6,7}$) and with those at each end ($L_{L,1}$ joining linker to β1 and $L_{\alpha,\beta}$ joining β8 to SBDα). Consistent with a recent NMR study[35], the linker makes extensive contacts with NBD (**Fig. 2b** and **Supplementary Figs. 1** and **7c**). These interactions are similar to those in Sse1-ATP, as previous mutational tests at Asn170, Thr173 and Val389 had indicated[23].

Conformations of SBDβ loops $L_{L,1}$, $L_{2,3}$ and $L_{4,5}$ in DnaK-ATP differ from those in Sse1-ATP, and this generates a number of novel contacts (**Supplementary Fig. 7a**,**b**). On $L_{L,1}$, Val394 and Leu397 make hydrophobic contacts with NBD (**Fig. 6a** and **Supplementary Fig. 7g**); and both Lys414 and Asn415 on $L_{2,3}$ form hydrogen bonds with Asp326 and Thr221 from NBD (**Fig. 6a** and **Supplementary Fig. 7h**), consistent with previous studies on essentiality for allosteric coupling[24,41]. Moreover, Ile418 from $L_{2,3}$ mediates hydrophobic interaction with the linker backbone. Gln442 on $L_{4,5}$ forms hydrogen bonds with Arg151 and Asp148 on NBD (**Fig. 6a** and **Supplementary Fig. 7i**). Mutational studies have implicated both Arg151 and Asp148 in allosteric coupling[42,43]. Loop $L_{6,7}$ is heavily involved in the NBD-SBDβ interface (**Fig. 6a** and **Supplementary Fig. 7d**) through Hsp70-conservative residues Asp481 and Ile483 interacting with highly conserved counterparts on NBD (Arg151, Gln152, Lys155 and Ile168). We have confirmed the functional importance of Asp481 and Ile483 in previous mutagenesis studies[23], and the functional importance of Gln152, Arg151 and Lys155 has been shown in other studies (refs. 34,43,44).

Both $L_{\alpha,\beta}$ and SBDα of DnaK change radically upon ATP binding, and the interface between NBD and $L_{\alpha,\beta}$ (NBD-$L_{\alpha,\beta}$) in particular is quite different between DnaK-ATP and Sse1-ATP. Whereas Asp159 forms a hydrogen bond with the α-β juncture in Sse1-ATP[23], a similar function is carried out by Asp100 in DnaK-ATP (**Fig. 6a** and **Supplementary Fig. 7e**). In keeping with this difference, Asp156 in DnaK (Asp159 in Sse1) was the only one of nine tested DnaK counterparts of Sse1-ATP interfacial residues that had a negligible phenotype.

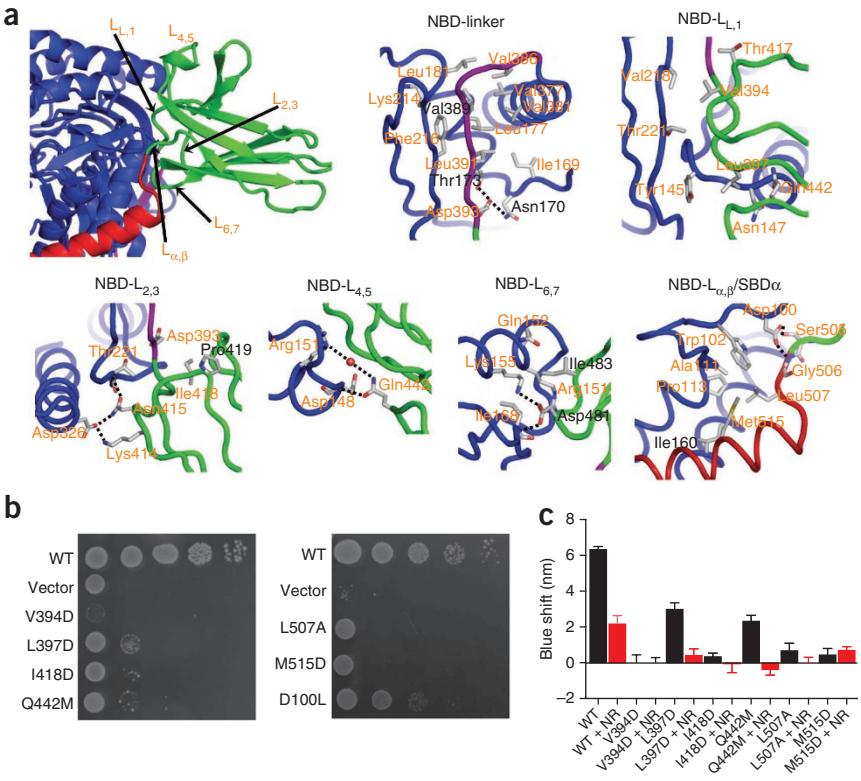

Figure 6 Characteristics of domain interfaces in DnaK-ATP. (**a**) Identification of NBD-contacting loops from SBDβ (top left; domain color assignments as in **Fig. 1a**), and associated details of each indicated contact (residues targeted for mutagenesis are labeled). Residues that were tested in the Sse1-ATP structure paper[23] are labeled in black. (**b**) Growth tests on interfacial mutant variants. Serial dilutions (10× column-by-column) of fresh cultures expressing the indicated mutant genes were spotted onto plates and grown at 37 °C. (**c**) ATP-induced tryptophan-fluorescence shifts. Shifts in maximum Trp102 fluorescence in the absence of peptide substrates (black) and after addition of 30 μM substrate peptide NR (red) are shown. For each protein, blueshift was averaged from five independent measurements from at least two purifications. Error bars, s.e.m. ($n = 5$).

NBD-SBDα interactions also differed substantially from those in Sse1-ATP (**Supplementary Fig. 7f**). Residue Ile160 was still central, interacting with several αA hydrophobes (Ile512, Met515, Leu550 and Ala519; **Supplementary Fig. 7f**) in keeping with mutational sensitivity at Ile160 (ref. 23); however, structural adjustments also engage Ala11, Trp102 and Pro113 with Leu507 and Met515 (**Fig. 6a** and **Supplementary Fig. 7j**).

To test the importance of previously unidentified contacts in allosteric coupling, we mutated key contact residues in DnaK: V394D, L397D, I418D, Q442M, L507A, M515D and D100L, each individually. These residues are highly conserved across Hsp70s (except for Asp100, which is conserved in prokaryotes and mitochondria) (**Supplementary Fig. 1**). As expected, all of these mutations compromised the *in vivo* activity of DnaK in growth tests (**Fig. 6b** and **Supplementary Fig. 6b**,**e**). To test whether the ATP-induced allosteric coupling was disrupted in these mutants, we purified each mutant variant (except D100L, which showed a moderate growth phenotype) and biochemically characterized allosteric coupling by tryptophan fluorescence assay. Each of the mutant proteins showed smaller blueshifts than the wild-type DnaK (**Fig. 6c**), confirming defects in ATP-induced allosteric coupling. Moreover, consistent with previous observations, addition of peptide substrate reduced blueshifts that remained substantial. In contrast, peptide substrate binding activity was largely intact in all mutants except I418D, even though all of the mutated residues were in SBD (**Supplementary Table 2**). Moreover, the functional importance of these residues is mostly preserved in yeast Hsp70 Ssa1 (**Supplementary Fig. 6c**,**d**). Thus, as for eight of nine putative DnaK-ATP interfacial contacts identified in Sse1-ATP, these additional contact residues are also essential for allosteric coupling.

Potential role of dimeric DnaK-ATP

The two almost-symmetric DnaK-ATP molecules in the crystal are associated with face-to-face contacts between NBDs and with each SBDα extending alongside NBD lobe II from its partner (**Fig. 2a**). This mode of association resembles that in the nucleotide-exchange heterodimer of Sse1 and human Hsp70 (ref. 45). The interfacial area between protomers is large (>3,000 Å^2) and shape complementarity is high (0.71) (**Supplementary Table 1**), indicating that the structure reflects a molecular dimer; however, dimerization of DnaK in solution was weak, with a dissociation constant (K_d) of 0.90 ± 0.16 mM (s.e.m) from sedimentation equilibrium analysis by analytical ultracentrifugation. The function of dimerization needs to be explored by future work.

DISCUSSION

The structure presented here for an intact Hsp70 in the ATP-bound state shows how ATP binding to NBD induces an opening of the polypeptide-binding channel in SBD (**Fig. 7**). In the ADP-bound state, Hsp70 has a high affinity for polypeptide substrates. When substrates bind, the polypeptide-binding channel closes and SBDα covers the polypeptide-binding site. Upon ATP-ADP exchange, Hsp70 is converted into the ATP-bound state, and the NBD and SBD form extensive contacts, which leads to radical conformational changes in SBD. The NBD pulls SBDα away from SBDβ, holds onto the $L_{1,2}$ side of the polypeptide-binding channel on SBDβ through $L_{L,1}$, $L_{2,3}$ and $L_{4,5}$ and then twists $L_{6,7}$ and $L_{\alpha,\beta}$. The distortions in $L_{6,7}$ and $L_{\alpha,\beta}$ propagate to the other side of the SBDβ, and then the $L_{3,4}$ side of the polypeptide-binding channel is flipped open to make the peptide-binding site more accessible. Subsequently, bound polypeptide substrate is released either to fold or to enter another round of the chaperone cycle. Associated biochemical and cellular tests support a mechanism whereby ATP binding causes release of polypeptide substrates. Conformational changes are transmitted through domain interfaces that are highly conserved across Hsp70s from different species and different cellular compartments. Moreover, our previous mutational tests[23] showed common essentialities between cytoplasmic yeast Hsp70 Ssa1 and bacterial Hsp70 DnaK, and this was also true here (**Fig. 6b** and **Supplementary Fig. 6c**,**d**). Thus, it is possible that the proposed allosteric mechanism for Hsp70 activity is universal.

The similarities between the DnaK-ATP and Sse1-ATP structures further confirmed that Hsp70s and Hsp110s are homologs. However, there are also substantial differences in both relative domain orientations and domain interfaces, and these differences could underlie their functional differences. Although peptide substrate binding in both Hsp70s and Hsp110s is ATP-sensitive, it is likely that they use different mechanisms, as the conformations of SBDβ are quite different in these two structures.

Allosteric coupling in Hsp70s is a two-way street: ATP binding effects polypeptide release, as we now better understand, but polypeptide re-binding strongly stimulates ATP hydrolysis. We anticipate further characterization of Hsp70-ATP in an ATPase-stimulating state (Qinglian Liu, R. Fan, J.Y., J.L.W., Qun Liu and W.A.H., unpublished data).

Three related publications have recently appeared. An NMR study shows that DnaK-ATP can have two alternative conformations[46]; the overall conformation of ATP in complex with DnaK in a disulfide bond–stabilized structure is similar to that seen here[47]; and we have published a detailed account of the native SAD phase evaluation for DnaK-ATP[48].

METHODS

Methods and any associated references are available in the online version of the paper.

Accession codes. Atomic coordinates and structure factors have been deposited in the Protein Data Bank under accession numbers 4JNF (DnaK SBD-L′$_{3,4}$), 4JNE (DnaK-ATP, native) and 4JN4 (DnaK-ATP, SAD).

Note: Supplementary information is available in the online version of the paper.

ACKNOWLEDGMENTS

We thank E. Craig, D. Logothetis, G. Tseng, L. Avery, L. Greene, J. Rife and C. Fox for critically reading the manuscript and providing insightful suggestions. We are grateful to J. Schwanof, R. Abramowitz and X. Yang (Brookhaven National Laboratory Beamline X4A and X4C) for their assistance in collecting diffraction data. We thank D. Kumar for technical support and C. Escalante for the PC1 photon counting spectrofluorimeter. This work was supported by startup funds from the Virginia Commonwealth University School of Medicine (to Qinglian Liu), a New Scholar Award in Aging from the Ellison Medical Foundation (AG-NS-0587-09 to Qinglian Liu) and a Grant-In-Aid Award from the American Heart Association (11GRNT7460003 to Qinglian Liu).

AUTHOR CONTRIBUTIONS

Qinglian Liu designed the study and experiments. Qinglian Liu and L.Z. screened, identified and carried out the cloning for the crystallization construct of

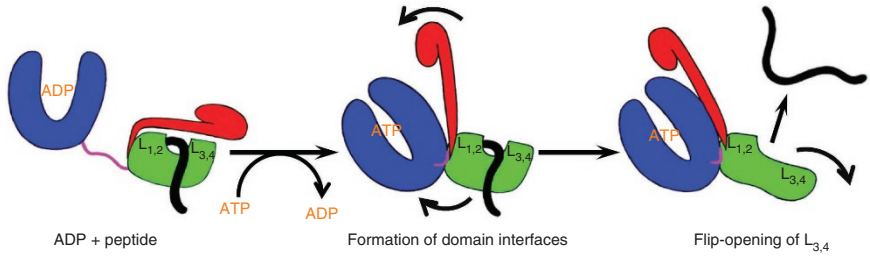

Figure 7 Model for allosteric opening of the polypeptide-binding site when an Hsp70 binds ATP. Hsp70 domain color assignments are as in **Figure 1a**. Polypeptide substrates are shown in black.

full-length DnaK. R.Q. and E.B.S. prepared the crystals for full-length DnaK and isolated SBD, respectively. Qun Liu and Qinglian Liu performed the structure determination and modeling. R.Q., E.B.S., K.Q.L., X.X., H.X., J.Y., J.L.W. and C.V. carried out the cloning of the mutations for biochemical analysis, protein purification, biochemical and genetic analysis. L.Z. performed computational analysis on the structures. Qinglian Liu, W.A.H. and L.Z. analyzed the structures, carried out data analysis and wrote the manuscript.

COMPETING FINANCIAL INTERESTS

The authors declare no competing financial interests.

1. Hartl, F.U., Bracher, A. & Hayer-Hartl, M. Molecular chaperones in protein folding and proteostasis. *Nature* **475**, 324–332 (2011).
2. Balch, W.E., Morimoto, R.I., Dillin, A. & Kelly, J.W. Adapting proteostasis for disease intervention. *Science* **319**, 916–919 (2008).
3. Bukau, B. & Horwich, A.L. The Hsp70 and Hsp60 chaperone machines. *Cell* **92**, 351–366 (1998).
4. Mayer, M.P. Gymnastics of molecular chaperones. *Mol. Cell* **39**, 321–331 (2010).
5. Zuiderweg, E.R. *et al.* Allostery in the Hsp70 Chaperone Proteins. *Top. Curr. Chem.* **328**, 99–153 (2013).
6. Rüdiger, S., Buchberger, A. & Bukau, B. Interaction of Hsp70 chaperones with substrates. *Nat. Struct. Biol.* **4**, 342–349 (1997).
7. Flaherty, K.M., DeLuca-Flaherty, C. & McKay, D.B. Three-dimensional structure of the ATPase fragment of a 70K heat-shock cognate protein. *Nature* **346**, 623–628 (1990).
8. Sriram, M., Osipiuk, J., Freeman, B., Morimoto, R. & Joachimiak, A. Human Hsp70 molecular chaperone binds two calcium ions within the ATPase domain. *Structure* **5**, 403–414 (1997).
9. Harrison, C.J., Hayer-Hartl, M., Di Liberto, M., Hartl, F. & Kuriyan, J. Crystal structure of the nucleotide exchange factor GrpE bound to the ATPase domain of the molecular chaperone DnaK. *Science* **276**, 431–435 (1997).
10. Jiang, J., Prasad, K., Lafer, E.M. & Sousa, R. Structural basis of interdomain communication in the Hsc70 chaperone. *Mol. Cell* **20**, 513–524 (2005).
11. Chang, Y.W., Sun, Y.J., Wang, C. & Hsiao, C.D. Crystal structures of the 70-kDa heat shock proteins in domain disjoining conformation. *J. Biol. Chem.* **283**, 15502–15511 (2008).
12. Zhu, X. *et al.* Structural analysis of substrate binding by the molecular chaperone DnaK. *Science* **272**, 1606–1614 (1996).
13. Wang, H. *et al.* NMR solution structure of the 21 kDa chaperone protein DnaK substrate binding domain: a preview of chaperone-protein interaction. *Biochemistry* **37**, 7929–7940 (1998).
14. Pellecchia, M. *et al.* Structural insights into substrate binding by the molecular chaperone DnaK. *Nat. Struct. Biol.* **7**, 298–303 (2000).
15. Liebscher, M. & Roujeinikova, A. Allosteric coupling between the lid and interdomain linker in DnaK revealed by inhibitor binding studies. *J. Bacteriol.* **191**, 1456–1462 (2009).
16. Buchberger, A. *et al.* Nucleotide-induced conformational changes in the ATPase and substrate binding domains of the DnaK chaperone provide evidence for interdomain communication. *J. Biol. Chem.* **270**, 16903–16910 (1995).
17. Swain, J.F. *et al.* Hsp70 chaperone ligands control domain association via an allosteric mechanism mediated by the interdomain linker. *Mol. Cell* **26**, 27–39 (2007).
18. Bertelsen, E.B., Chang, L., Gestwicki, J.E. & Zuiderweg, E.R. Solution conformation of wild-type *E. coli* Hsp70 (DnaK) chaperone complexed with ADP and substrate. *Proc. Natl. Acad. Sci. USA* **106**, 8471–8476 (2009).
19. Schmid, D., Baici, A., Gehring, H. & Christen, P. Kinetics of molecular chaperone action. *Science* **263**, 971–973 (1994).
20. Flynn, G.C., Chappell, T.G. & Rothman, J.E. Peptide binding and release by proteins implicated as catalysts of protein assembly. *Science* **245**, 385–390 (1989).
21. Flaherty, K.M., Wilbanks, S.M., DeLuca-Flaherty, C. & McKay, D.B. Structural basis of the 70-kilodalton heat shock cognate protein ATP hydrolytic activity. II. Structure of the active site with ADP or ATP bound to wild type and mutant ATPase fragment. *J. Biol. Chem.* **269**, 12899–12907 (1994).
22. Jiang, J. *et al.* Structural basis of J cochaperone binding and regulation of Hsp70. *Mol. Cell* **28**, 422–433 (2007).
23. Liu, Q. & Hendrickson, W.A. Insights into Hsp70 chaperone activity from a crystal structure of the yeast Hsp110 Sse1. *Cell* **131**, 106–120 (2007).
24. Smock, R.G. *et al.* An interdomain sector mediating allostery in Hsp70 molecular chaperones. *Mol. Syst. Biol.* **6**, 414 (2010).
25. Mapa, K. *et al.* The conformational dynamics of the mitochondrial Hsp70 chaperone. *Mol. Cell* **38**, 89–100 (2010).
26. Marcinowski, M. *et al.* Substrate discrimination of the chaperone BiP by autonomous and cochaperone-regulated conformational transitions. *Nat. Struct. Mol. Biol.* **18**, 150–158 (2011).
27. Schlecht, R., Erbse, A.H., Bukau, B. & Mayer, M.P. Mechanics of Hsp70 chaperones enables differential interaction with client proteins. *Nat. Struct. Mol. Biol.* **18**, 345–351 (2011).
28. McCarty, J.S. & Walker, G.C. DnaK as a thermometer: threonine-199 is site of autophosphorylation and is critical for ATPase activity. *Proc. Natl. Acad. Sci. USA* **88**, 9513–9517 (1991).
29. Osipiuk, J., Georgopoulos, C. & Zylicz, M. Initiation of lambda DNA replication. The *Escherichia coli* small heat shock proteins, DnaJ and GrpE, increase DnaK's affinity for the lambda P protein. *J. Biol. Chem.* **268**, 4821–4827 (1993).
30. Xu, X. *et al.* The unique peptide substrate binding properties of 110 KDA heatshock protein (HSP110) determines its distinct chaperone activity. *J. Biol. Chem.* **287**, 5661–5672 (2012).
31. Smock, R.G., Blackburn, M.E. & Gierasch, L.M. Conserved, disordered C terminus of DnaK enhances cellular survival upon stress and DnaK *in vitro* chaperone activity. *J. Biol. Chem.* **286**, 31821–31829 (2011).
32. Liu, Q. *et al.* Structures from anomalous diffraction of native biological macromolecules. *Science* **336**, 1033–1037 (2012).
33. Swain, J.F. & Gierasch, L.M. The changing landscape of protein allostery. *Curr. Opin. Struct. Biol.* **16**, 102–108 (2006).
34. Vogel, M., Mayer, M.P. & Bukau, B. Allosteric regulation of Hsp70 chaperones involves a conserved interdomain linker. *J. Biol. Chem.* **281**, 38705–38711 (2006).
35. Zhuravleva, A. & Gierasch, L.M. Allosteric signal transmission in the nucleotide-binding domain of 70-kDa heat shock protein (Hsp70) molecular chaperones. *Proc. Natl. Acad. Sci. USA* **108**, 6987–6992 (2011).
36. Kumar, D.P. *et al.* The four hydrophobic residues on the Hsp70 inter-domain linker have two distinct roles. *J. Mol. Biol.* **411**, 1099–1113 (2011).
37. Bhattacharya, A. *et al.* Allostery in Hsp70 chaperones is transduced by subdomain rotations. *J. Mol. Biol.* **388**, 475–490 (2009).
38. Rist, W., Graf, C., Bukau, B. & Mayer, M.P. Amide hydrogen exchange reveals conformational changes in hsp70 chaperones important for allosteric regulation. *J. Biol. Chem.* **281**, 16493–16501 (2006).
39. Swain, J.F., Schulz, E.G. & Gierasch, L.M. Direct comparison of a stable isolated Hsp70 substrate-binding domain in the empty and substrate-bound states. *J. Biol. Chem.* **281**, 1605–1611 (2006).
40. Lovell, S.C. *et al.* Structure validation by Calpha geometry: phi,psi and Cbeta deviation. *Proteins* **50**, 437–450 (2003).
41. Montgomery, D.L., Morimoto, R.I. & Gierasch, L.M. Mutations in the substrate binding domain of the *Escherichia coli* 70 kDa molecular chaperone, DnaK, which alter substrate affinity or interdomain coupling. *J. Mol. Biol.* **286**, 915–932 (1999).
42. Gässler, C.S. *et al.* Mutations in the DnaK chaperone affecting interaction with the DnaJ cochaperone. *Proc. Natl. Acad. Sci. USA* **95**, 15229–15234 (1998).
43. Vogel, M., Bukau, B. & Mayer, M.P. Allosteric regulation of Hsp70 chaperones by a proline switch. *Mol. Cell* **21**, 359–367 (2006).
44. Davis, J.E., Voisine, C. & Craig, E.A. Intragenic suppressors of Hsp70 mutants: interplay between the ATPase- and peptide-binding domains. *Proc. Natl. Acad. Sci. USA* **96**, 9269–9276 (1999).
45. Polier, S., Dragovic, Z., Hartl, F.U. & Bracher, A. Structural basis for the cooperation of Hsp70 and Hsp110 chaperones in protein folding. *Cell* **133**, 1068–1079 (2008).
46. Zhuravleva, A., Clerico, E.M. & Gierasch, L.M. An interdomain energetic tug-of-war creates the allosterically active state in Hsp70 molecular chaperones. *Cell* **151**, 1296–1307 (2012).
47. Kityk, R., Kopp, J., Sinning, I. & Mayer, M.P. Structure and dynamics of the ATP-bound open conformation of Hsp70 chaperones. *Mol. Cell* **48**, 863–874 (2012).
48. Liu, Q., Liu, Q. & Hendrickson, W.A. Robust structural analysis of native biological macromolecules from multi-crystal anomalous diffraction data. *Acta Crystallogr. D Biol. Crystallogr.* (in the press).

ONLINE METHODS

Protein expression and purification. The DnaK-T199A $L'_{3,4}$ (residues 2–610) and SBD-$L'_{3,4}$ (residues 388–610) constructs were cloned into a pSMT3 vector and expressed as Smt3 fusion proteins in *E. coli* BL21(DE3) Gold cells. pSMT vector is a generous gift from C. Lima[49]. The fusion proteins were first purified on a HisTrap column. After the Smt3 tag was removed by Ulp1 protease, the DnaK proteins were separated from the Smt3 tag using a HisTrap column and further purified using a HiTrap Q and Superdex 200 16/60 column. The Ulp1 cleavage introduces a serine residue, effectively generating an M1S mutation. All the columns are from GE Healthcare. The purified proteins were concentrated to 30–50 mg/ml in a buffer containing 5 mM HEPES-KOH (pH 7.5) and 10 mM KCl and flash frozen in liquid nitrogen.

All of the DnaK mutant proteins used in the biochemical assays were cloned into the *dnak* expression plasmid pBB46 and expressed in the *dnak* deletion strain BB205 ($cam^R kan^R$)[50]. To facilitate purification, a His_6 tag was fused to the C terminus (addition of this tag has no observable influence on the *in vivo* function of DnaK). Proteins were purified as described previously[36]. Briefly, after being purified by HisTrap column, each protein was further purified on a HiTrap Q column. Before being flash frozen in liquid nitrogen, each protein was concentrated to 10–50 mg/ml. The purification of DnaJ and GrpE was essentially as described previously[30,37].

Crystallization, data collection and model building. For the DnaK-T199A $L'_{3,4}$ protein, crystals were grown at 4 °C in 1.8–2.0 M $(NH_4)_2SO_4$, 0.1 M HEPES-NaOH (pH 7.5) and 2–3% polyethylene glycol (PEG) 400. Crystals of SBD-$L'_{3,4}$ were grown at 20 °C in 2.0 M $(NH_4)_2SO_4$, and 0.1 M Tris-HCl (pH 8.5). Both crystals were cryoprotected with 15% glycerol in mother liquor and flash frozen in liquid nitrogen. All diffraction data sets were collected at the X4A and X4C beamlines of the National Synchrotron Light Source at Brookhaven National Laboratory. To enhance anomalous signals from native DnaK-T199A $L'_{3,4}$ crystals, we tuned the wavelength of beamline X4A to the Fe K-edge (λ = 1.743 Å, E = 7.112 keV) as verified by fluorescence scan. Anomalous diffraction data sets from five crystals were integrated by XDS[51] and scaled by SCALA[52]. We collected and processed a higher-resolution native data set at a wavelength of 0.979 Å using beamline X4C. Data collection and reduction statistics for native and multi-crystal single-wavelength anomalous diffraction (SAD) data sets are listed in **Table 1**.

We used the multi-crystal native-SAD method[32] for structure determination based on S, P and Mg anomalous scatterers (51 sites for 1,212 residues). Briefly, we enhanced anomalous signals by analyzing, scaling and merging anomalous signals from five crystals. Anomalous scatter substructure was determined by SHELXD[53]. The substructure was refined and completed for phase calculation using Phaser[54]. The phases were then density modified by DM[55] to break the phase ambiguity, and this resulted in electron density maps of sufficient quality for automated model building with Arp/wArp[56]. Although noncrystallographic two-fold symmetry is present, such information was not required for native-SAD phasing. Further refinement and model building were carried out using Phenix[57] and COOT[58]. Multi-crystal SAD data and the 1.96-Å resolution native data were used for refinements. The refined model was validated by PROCHECK[59] and Molprobity[60] to assess geometry. All residues are in favored regions with no Ramachandran outliers.

To solve the structure of SBD-$L'_{3,4}$, a diffraction data set at 1.62-Å resolution from a single crystal was collected at wavelength 0.979 Å at Beamline X4C, integrated and scaled by HKL2000 (ref. 61). The structure was solved by molecular replacement using the structure of isolated DnaK SBD (1DKZ) as search model. Model building, refinement and validation of SBD-$L'_{3,4}$ followed the same protocol as for the full-length DnaK.

Tryptophan fluorescence assay. The assay was performed as described previously[36]. Briefly, DnaK proteins were diluted to 1 µM in buffer A (25 mM HEPES-KOH (pH 7.5), 100 mM KCl, 10 mM magnesium acetate, 10% glycerol and 2 mM DTT). ATP or ADP (5 µl 200 mM) was added to 1 ml DnaK protein solution, and the mixture was incubated for 2 min. Emission spectra were collected from 310 nm to 400 nm on a PC1 Photon Counting Spectrofluorimeter from ISS (Illinois, USA) with an excitation wavelength of 295 nm. The peak reading of the ADP spectrum of each protein was set as 1, and the relative fluorescence was plotted versus wavelength. The blueshift for each protein was calculated as the difference in emission maximums between the spectra in the presence and absence of ATP.

Site-directed mutagenesis and growth tests. All DnaK and Ssa1 mutations were introduced using the QuikChange Lightening Site-directed Mutagenesis kit (Stratagene). Growth tests were performed as described previously[23], with some modifications. For growth tests in DnaK, pBB46 plasmids (amp^R) carrying mutant *dnak* were transformed into a *dnak* deletion strain BB205 ($cam^R kan^R$)[50]. Because *E. coli* growth is dependent on a functional DnaK at 37 °C but not at 30 °C, growth tests were carried out at 37 °C, and control tests were performed at 30 °C. For each mutant, a fresh overnight culture was prepared from a fresh transformation. Five-microliter serial dilutions of the overnight cultures were spotted on LB plates containing 50 µg/ml ampicillin, 25 µg/ml kanamycin, 25 µg/ml chloramphenicol and 20 µM IPTG and incubated overnight at 37 °C to evaluate growth.

All of the Ssa1 mutants were cloned into an Ssa1-expressing plasmid, pRS313-SSA1, and transformed into a *SSA1* mutant yeast strain *JB67* (ref. 62). Besides harboring deletions of *SSA2-4*, *JB67* carries a temperature-sensitive *SSA1* mutant, *ssa1-45*, and thus is unable to grow at 37 °C. Ten-microliter serial dilutions of fresh overnight cultures from fresh transformations were spotted onto yeast minimum medium plates lacking histidine. Growth was scored after incubating at 37 °C for 2–3 d. Growth tests at 30 °C were used as controls.

Luciferase refolding assay. Purified firefly luciferase was purchased from Promega. Before denaturing at 42 °C for 20 min, luciferase was diluted in buffer B (25 mM HEPES-KOH (pH 7.5) 100 mM KCl, 10 mM magnesium acetate, 2 mM DTT and 3 mM ATP) to a final concentration of 100 nM in the presence of indicated DnaK proteins (3 µM). To start refolding reactions, a reaction mixture containing DnaK (3 µM), DnaJ (0.67 µM) and GrpE (0.33 µM) was added to heat-denatured luciferase. At indicated time points, 2 µl of refolding reaction was mixed with 50 µl luciferase substrate, and luciferase activity was read in a Berthold LB9507 luminometer.

Fluorescence anisotropy assay of peptide substrate binding affinity and kinetics. NR peptide (sequence: NRLLLTG) labeled with fluorescein at the N terminus (F-NR) was obtained at purity >95% from NEOBioscience. To determine binding affinity, serial dilutions of DnaK proteins were incubated with F-NR (20 nM final concentration) in buffer A for at least 3 h to reach equilibrium. Fluorescence anisotropy measurements were carried out on a Beacon 2000 instrument (Invitrogen). To calculate dissociation constants (K_d), data were fitted to a one-site binding equation using PRISM (GraphPad, http://www.graphpad.com/prism/). Each sample was read at least three times, and each DnaK protein was repeated at least two times with more than two different protein preparations. For binding-kinetics measurements, 10 µM of DnaK protein was incubated with indicated nucleotide for 2 min, then F-NR was added to start the binding reaction. Anisotropy was read every 10 s.

Molecular dynamic simulation analysis. Molecular dynamic (MD) simulations were carried out using GROMACS[63]. Simulations for each structure were carried out for 20 ns without consideration of crystal contacts or symmetry mates. Principal component analysis with G_COVAR[64] on the conformations collected by MD simulations was used to calculate the raw covariance matrix in three dimensions for each pair of Cα atoms. To systematically survey the strength of all contacts, we used the normalized covariance factor (scale, 0–1), which is also called cross-correlation[65]. The higher the normalized covariance factor, the more stable a contact is.

49. Mossessova, E. & Lima, C.D. Ulp1-SUMO crystal structure and genetic analysis reveal conserved interactions and a regulatory element essential for cell growth in yeast. *Mol. Cell* **5**, 865–876 (2000).
50. Burkholder, W.F. *et al.* Mutations in the C-terminal fragment of DnaK affecting peptide binding. *Proc. Natl. Acad. Sci. USA* **93**, 10632–10637 (1996).
51. Kabsch, W. XDS. *Acta Crystallogr. D Biol. Crystallogr.* **66**, 125–132 (2010).
52. Evans, P.R. An introduction to data reduction: space-group determination, scaling and intensity statistics. *Acta Crystallogr. D Biol. Crystallogr.* **67**, 282–292 (2011).
53. Schneider, T.R. & Sheldrick, G.M. Substructure solution with SHELXD. *Acta Crystallogr. D Biol. Crystallogr.* **58**, 1772–1779 (2002).
54. Read, R.J. & McCoy, A.J. Using SAD data in Phaser. *Acta Crystallogr. D Biol. Crystallogr.* **67**, 338–344 (2011).

doi:10.1038/nsmb.2583

55. Cowtan, K.D. & Zhang, K.Y.J. Density modification for macromolecular phase improvement. *Prog. Biophys. Mol. Biol.* **72**, 245–270 (1999).
56. Langer, G., Cohen, S.X., Lamzin, V.S. & Perrakis, A. Automated macromolecular model building for X-ray crystallography using ARP/wARP version 7. *Nat. Protoc.* **3**, 1171–1179 (2008).
57. Adams, P.D. *et al.* The Phenix software for automated determination of macromolecular structures. *Methods* **55**, 94–106 (2011).
58. Emsley, P. & Cowtan, K. Coot: model-building tools for molecular graphics. *Acta Crystallogr. D Biol. Crystallogr.* **60**, 2126–2132 (2004).
59. Laskowski, R.A., Macarthur, M.W., Moss, D.S. & Thornton, J.M. PROCHECK: a program to check the stereochemical quality of protein structures. *J. Appl. Cryst.* **26**, 283–291 (1993).
60. Chen, V.B. *et al.* MolProbity: all-atom structure validation for macromolecular crystallography. *Acta Crystallogr. D Biol. Crystallogr.* **66**, 12–21 (2010).
61. Otwinowski, Z. & Minor, W. Processing of X-ray diffraction data collected in oscillation mode. *Methods Enzymol.* **276**, 307–326 (1997).
62. Becker, J., Walter, W., Yan, W. & Craig, E.A. Functional interaction of cytosolic hsp70 and a DnaJ-related protein, Ydj1p, in protein translocation *in vivo*. *Mol. Cell Biol.* **16**, 4378–4386 (1996).
63. Lindahl, E., Hess, B. & van der Spoel, D. GROMACS 3.0: a package for molecular simulation and trajectory analysis. *J. Mol. Model.* **7**, 306–317 (2001).
64. Balsera, M.A., Wriggers, W., Oono, Y. & Schulten, K. Principal component analysis and long time protein dynamics. *J. Phys. Chem.* **100**, 2567–2572 (1996).
65. Ichiye, T. & Karplus, M. Collective motions in proteins: a covariance analysis of atomic fluctuations in molecular dynamics and normal mode simulations. *Proteins* **11**, 205–217 (1991).